

Electronic Supplementary Information

A novel hydroxylamine ionic liquid salt resulting from the stabilization of NH₂OH by a SO₃H-functionalized ionic liquid

Zhihui Li^{a, b}, Qiusheng Yang^a, Xudong Qi^b, Yuanyuan Xu^a, Dongsheng Zhang^{a,*}, Yanji Wang^{a,*} and Xinqiang Zhao^a

a Hebei Provincial Key Lab of Green Chemical Technology and High Efficient Energy Saving

Hebei University of Technology

Guang Rong Dao 8, Hongqiao Distric, Tianjin 300130 (China)

E-Mail: yjwang@hebut.edu.cn; zds1301@hebut.edu.cn

b School of Energy and Environmental Engineering

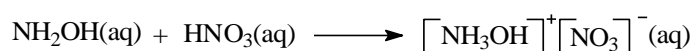
Hebei University of Technology

Tianjin 300401 (China)

Experimental Section

Materials and methods: Several Zn-based compounds, such as ZnO, ZnCl₂, ZnSO₄ and Zn(OAc)₂, were obtained commercially and tested as catalyst. All other chemicals (AR grade) were commercially available and used without further purification. The melting point was determined on a WRS-1B numeral melting point instrument. Element analysis was conducted with a Flash EA1112 elemental analyzer. FTIR spectra were recorded on a Bruker Vector 22 FTIR spectrometer in the 4000-400 cm⁻¹ range using liquid film or KBr tablet. A DXR Raman Microscope (Thermo Scientific) with a 532 nm excitation laser was used to record the Raman spectra. The ¹H NMR spectra were recorded on a Bruker AMX FT 400 MHz NMR spectrometer using D₂O and DMSO-d₆ as solvents, and the chemical shifts were expressed in ppm. The ¹³C NMR spectra were recorded on a Varian InfinityPlus 300 MHz superconducting fourier transform solid nuclear magnetic resonance spectrometry. TG was carried out on a SDT Q600 simultaneous DSC-TGA instrument at 10 K/min heating rate under a flow of air. In situ IR study was conducted on a React IRTM IC10 online reaction analysis system (METTLER TOLEDO), equipped with a light conduit and DiComp (diamond composite) insertion probe in the wave number range between 4000 and 650 cm⁻¹ and a resolution of 8 cm⁻¹.

Preparation of hydroxylamine ionic liquid salt ((NH₂OH)₂ IL): Free hydroxylamine is a weak alkali that has a small dissociation constant. It mainly exists in the form of NH₂OH in water.¹ The outermost orbit of N in NH₂OH has a lone pair of electrons that can easily combine with H⁺ released by an acid to form NH₃OH⁺. The coexistence of NH₃OH⁺ and the acid radical ion constitutes a hydroxylamine salt solution. Most of the aqueous hydroxylamine nitrate used as the new monopropellants are obtained via a controlled reaction (Scheme S1) between aqueous solution of hydroxylamine and nitric acid.² According to the preparation of hydroxylamine nitrate, acid IL was used (instead of nitric acid) to react with the aqueous solution of hydroxylamine to obtain a novel hydroxylamine IL salt.



Scheme S1 Formation reaction of hydroxylamine nitrate

1-Sulfobutyl-3-methyl imidazole hydrosulfate (IL) ([HSO₃-bmim][HSO₄], 46.1 mmol) was added into a 250 mL three-necked flask equipped with a dropping funnel and a stirrer. The flask was then placed in a low-temperature reaction bath, and the temperature was continuously kept under 2 °C. The aqueous solution of hydroxylamine (115.3 mmol) was added dropwise to the three-necked flask that contained the IL while stirring. When the neutralization process was completed, a clear solution was obtained. The clear solution was evaporated to dryness under reduced pressure to obtain the white (NH₂OH)₂ IL solid. The aqueous solution of hydroxylamine was obtained from a laboratory-made solution, which was prepared according to literature.^{2b} The acidic IL 1-sulfobutyl-3-methyl imidazolium hydrosulfate was synthesized according to previous literature.³

One-step synthesis of caprolactam: The reaction was performed in a 10 mL single-necked flask equipped with a magnetic stirrer. Typically, cyclohexanone (CYC), (NH₂OH)₂ IL and ZnCl₂ were charged into the flask, which was then sealed. No other additional solvent was required. The reaction mixture was heated in an oil bath at 130–160 °C and kept for 0.5–2.5 h. At the end of the reaction, the resulting mixture was cooled and then extracted twice with 3 mL of methylene dichloride. The obtained organic phase was identified by comparing their retention time with those

of authentic samples and by a Thermo Trace DSQ gas chromatography mass spectrometer. The concentrations of organic components were analyzed with a SP-3420 gas chromatograph.

In situ IR reaction: The in situ IR reaction was performed in a 50 mL three-necked flask equipped with a stirrer. In order to immerge the probe into the reaction solution, all of the raw materials used are magnified 20 times. CYC (20 mmol) was charged into the flask and heated in an oil bath to 150 °C, then ZnCl₂ (40 mmol) and (NH₂OH)₂ IL (40 mmol) were added into the flask, which was then sealed. The reaction mixture with the online reaction analysis system was then kept 150 °C for 2 h.

Recovery of the IL: To determine whether the IL combined in the (NH₂OH)₂ IL can be recovered, a one-step synthesis of caprolactam (CPL) was carried out under the optimal reaction conditions. After the completion of the reaction, the resulting mixture was cooled and extracted twice with methylene dichloride, and the raffinate phase was dissolved in water. A small amount of solid was separated by centrifugal separation, and the obtained aqueous solution was distilled with a rotary evaporator under vacuum to recover the IL.

Characterization data

Table S1 Species and corresponding frequency values of the (NH₂OH)₂ IL (Raman spectra)

Species	Frequency (cm ⁻¹)
N-OH stretch	1024
OH bend, NH ₃ rock	1190
NH ₃ deformation	1623
NH ₃ , rock + deformation (overtone)	2730
NH ₃ stretch	2965
OH stretch	3151

Fig. S1a-d ¹H and ¹³C-NMR spectra of the (NH₂OH)₂ IL and IL

IL: δ H (400 MHz; D₂O) 1.584(m, 2H), 1.860(t, 2H), 2.784(m, 2H), 3.730(d, 3H), 4.086(m, 2H), 7.277(d, 1H), 7.335(d, 1H), 8.575(s, 1H).

(NH₂OH)₂ IL: δ H (400 MHz; D₂O) 1.645(t, 2H), 1.926(t, 2H), 2.851(t, 2H), 3.795(s, 3H), 4.152(t, 2H), 7.344(s, 1H), 7.401(s, 1H), 8.649(s, 1H).

(NH₂OH)₂ IL: δ H (400 MHz; DMSO-d₆) 1.532(m, 2H), 1.873(m, 2H), 2.480(m, 2H), 3.855(s, 3H), 4.182(t, 2H), 7.713(t, 1H), 7.781(t, 1H), 8~9(bs, 5H), 9.160(s, 1H).

(NH₂OH)₂ IL: δ C (300 MHz, solid) 24.5, 27.1, 36.3, 50.7, 52.8, 122.0, 124.0, 139.0.

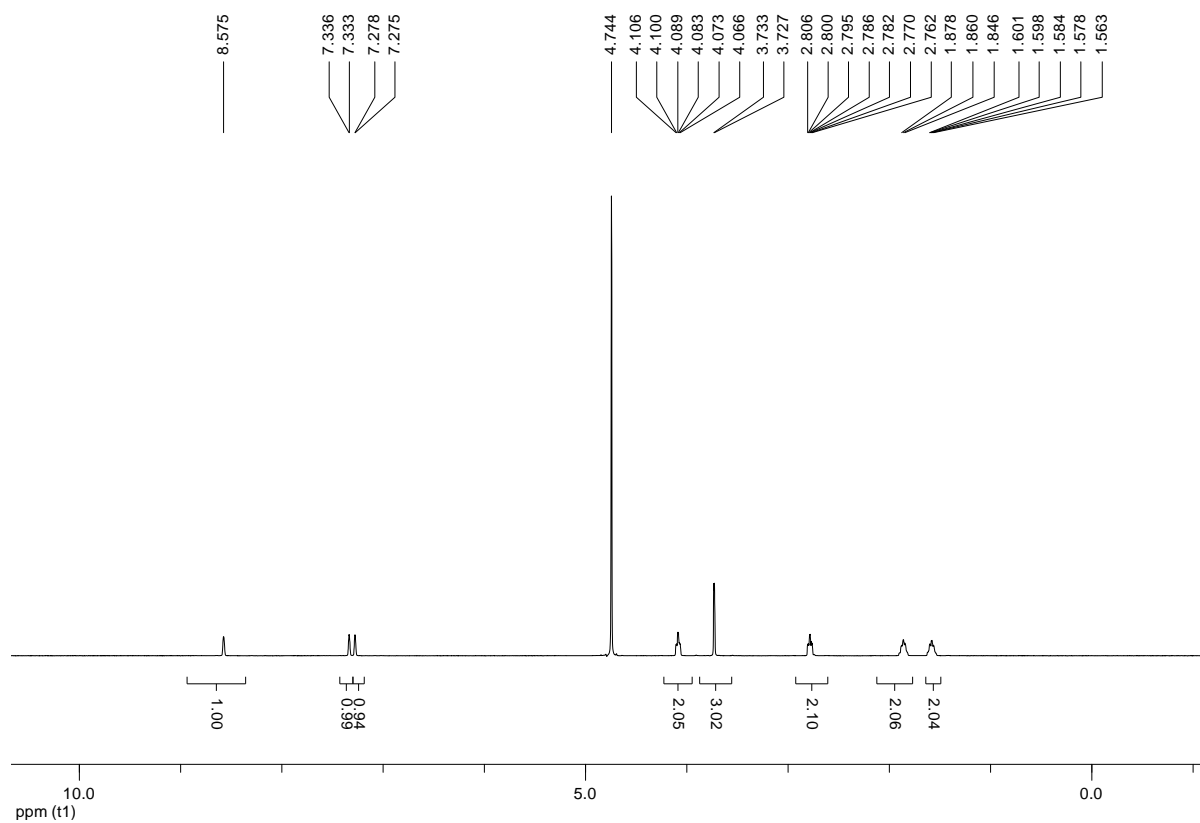


Fig. S1 (a) $^1\text{H-NMR}$ spectra of the IL (D_2O)

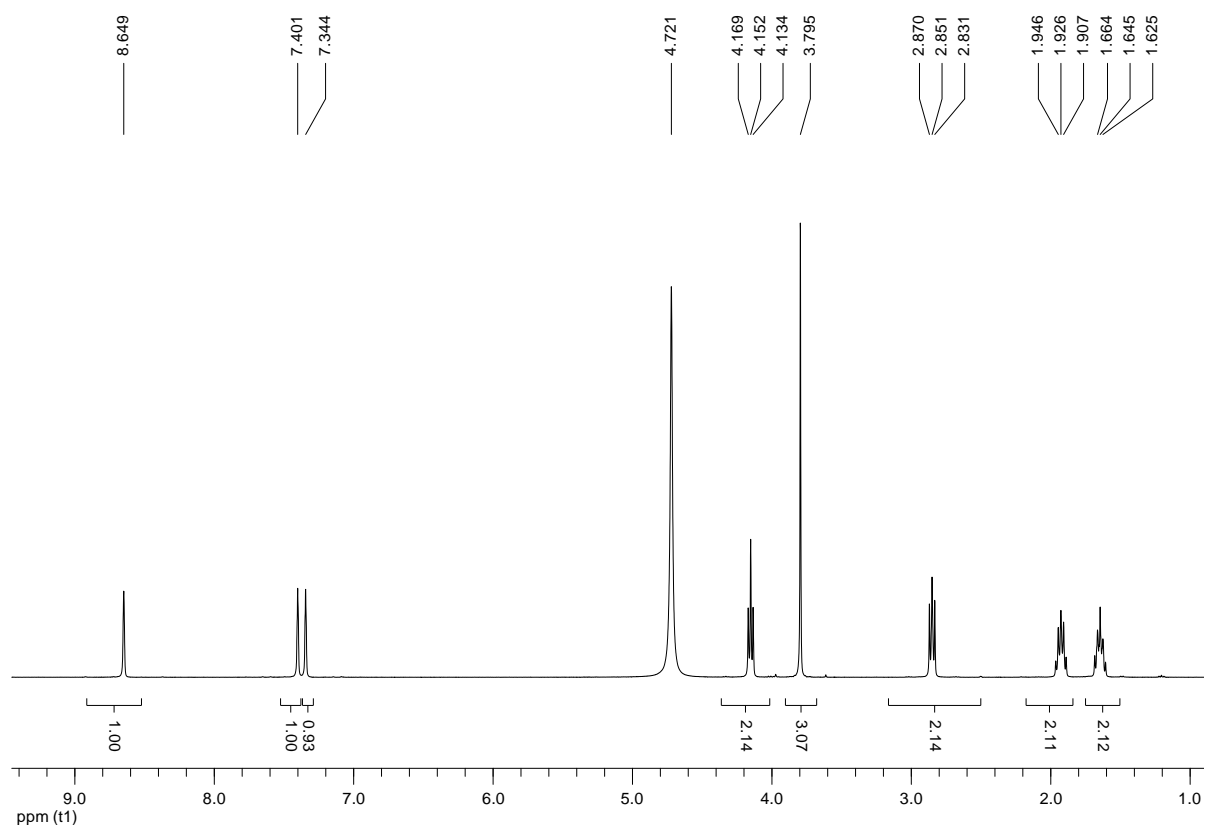


Fig. S1 (b) $^1\text{H-NMR}$ spectra of the $(\text{NH}_2\text{OH})_2$ IL (D_2O)

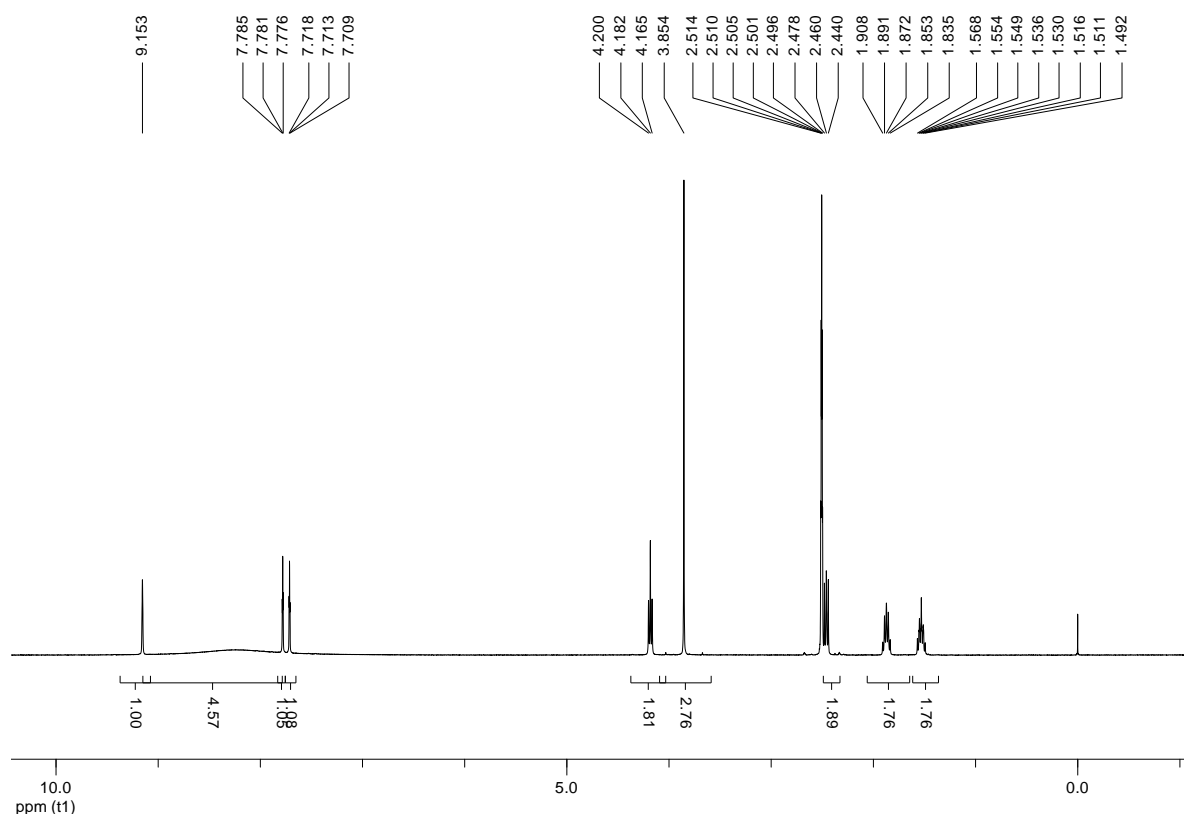


Fig. S1 (c) ^1H -NMR spectra of the $(\text{NH}_2\text{OH})_2$ IL (DMSO- d_6)

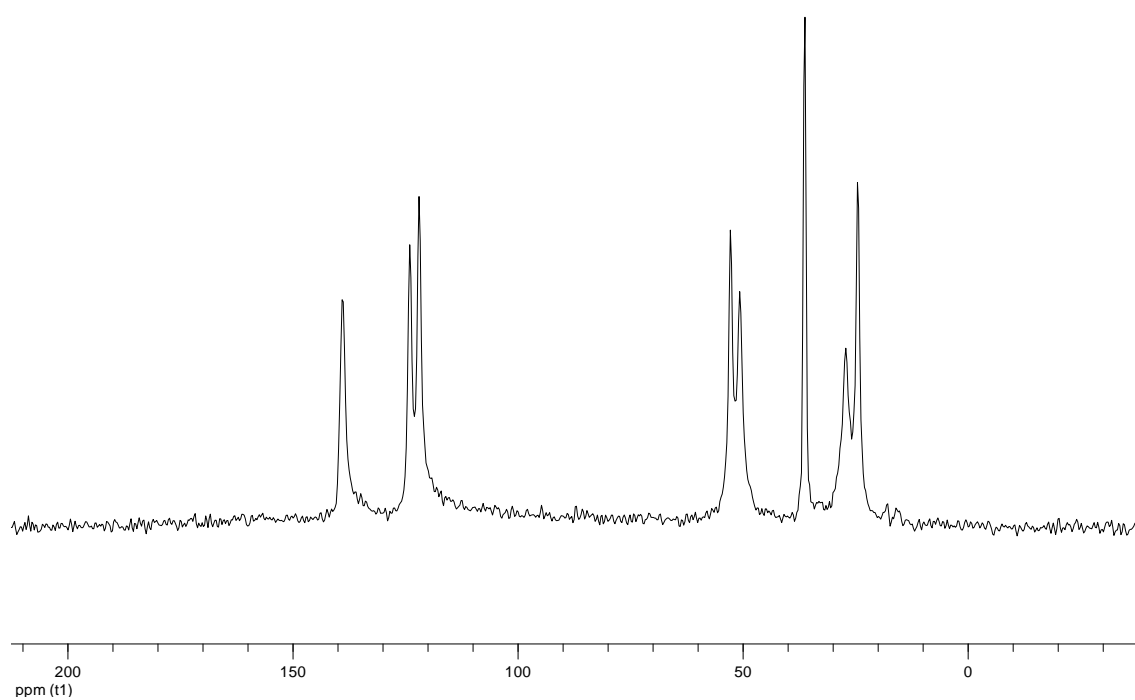


Fig. S1 (d) ^{13}C -NMR spectra of the $(\text{NH}_2\text{OH})_2$ IL

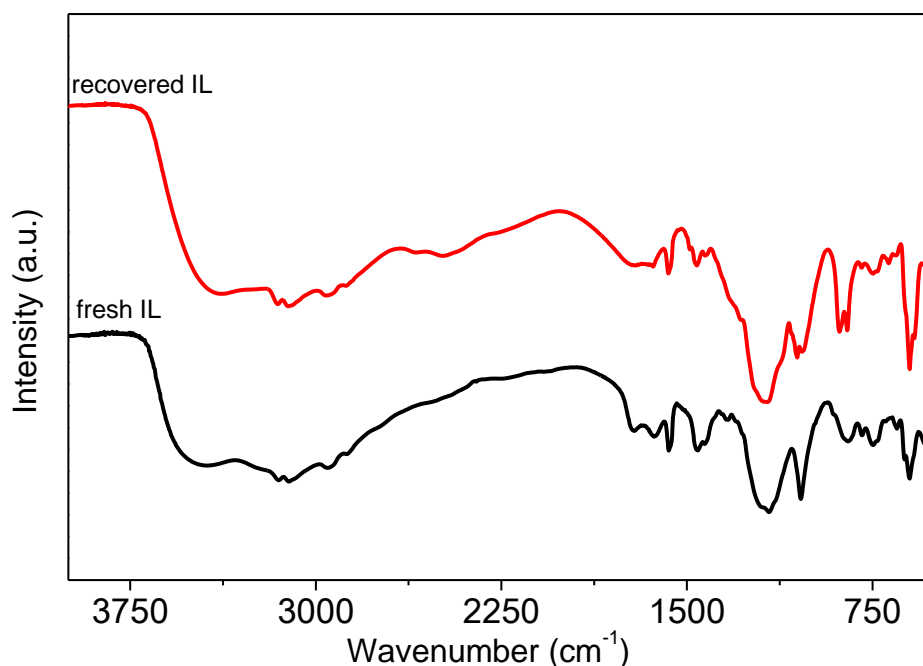


Fig. S2 FTIR spectra of the recovered and fresh IL

Computational details

Density functional theory (DFT) calculations were performed using a M062X hybrid functional with the Gaussian 09 program package.⁴ This M062X method has been confirmed to be appropriate for hydroxylamine and ionic liquids system in a number of previous studies.⁵ The geometries of each reactant involved in the reaction were fully optimized at the level of 6-31++ G in the gas phase. Frequency analyses were conducted with the same basis set to confirm that the optimized structures were ground states without imaginary frequency.⁶ In addition, the geometric parameters and electrostatic potentials were determined, and Natural bond orbital (NBO) and Mayer bond orders analysis were performed for the optimized structures of imidazole-containing ionic liquids.⁷ The interaction energy (ΔE) between NH_4O^+ and the other part anion was calculated with the correction for the basis set superposition error (BSSE) using the counterpoise method. If not noted otherwise, all thermodynamic data reported in this article were estimated at 25 °C under 1 atm and relative energies that refer to those with zero point energy correction.

Initially, geometry optimizations and vibrational frequency calculations were carried out on NH_2OH , $[\text{HSO}_3\text{-bmim}]\cdot\text{HSO}_4$ and $(\text{NH}_2\text{OH})_2$ IL using the M062X functional with 6-31++ G basis sets for all the atoms. The optimized structures of the above substances were confirmed as energy minima by frequency calculations. The electrostatic potential surfaces of the structures were constructed and are shown in Fig. S3a-g, where the red and blue colors indicate the negative and positive regions, respectively. Their coordinates are shown in Table S2I-V.

Obviously, the two main components of $(\text{NH}_2\text{OH})_2$ IL were NH_2OH and $[\text{HSO}_3\text{-bmim}]\cdot\text{HSO}_4$. As displayed in Fig. S3a, the main region of NH_2OH was positive and the negative region was located close to O and away from N because of their lone pairs and strong electronegative nature. For the ionic liquid of $[\text{HSO}_3\text{-bmim}]\cdot\text{HSO}_4$ (Fig. S3b), the two distinct regions were shown as

follows: the half region near the carbon chain and imidazole ring was positive, whereas the other half was negative and focused on the oxygen-rich region. These maps indicate that the interaction between the two substances took place mainly between the positive region of NH_2OH and the negative region of $[\text{HSO}_3\text{-bmim}]\cdot\text{HSO}_4$ (Fig. S3c). Moreover, two NH_2OH molecules can also be inserted into the oxygen-containing groups by three additional ways (denoted as $(\text{NH}_2\text{OH})_2$ ILs-2, -3, and -4; Fig. S3d-f). According to their relative Gibbs free energies, their stabilities can be arranged as follows: $(\text{NH}_2\text{OH})_2$ IL $>$ $(\text{NH}_2\text{OH})_2$ IL-2 $>$ $(\text{NH}_2\text{OH})_2$ IL-3 $>$ $(\text{NH}_2\text{OH})_2$ IL-4. Therefore, the structure of $(\text{NH}_2\text{OH})_2$ IL is most stable because of the small gaps and uniform distribution of the electrostatic potential, that is, one NH_2OH molecule in $(\text{NH}_2\text{OH})_2$ IL connected primarily with HSO_4^- , and another connected with both HSO_4^- and SO_3H . In addition, charge neutralization may not occur if the methylene groups and NH_2OH molecules were located in the different surfaces of the imidazole ring ($(\text{NH}_2\text{OH})_2$ IL-5, Fig. S2g). Meanwhile, the energy increased by 5.23 kcal/mol. Based on the above analysis, the optimal structure of the hydroxylamine IL salt is $(\text{NH}_2\text{OH})_2$ IL.

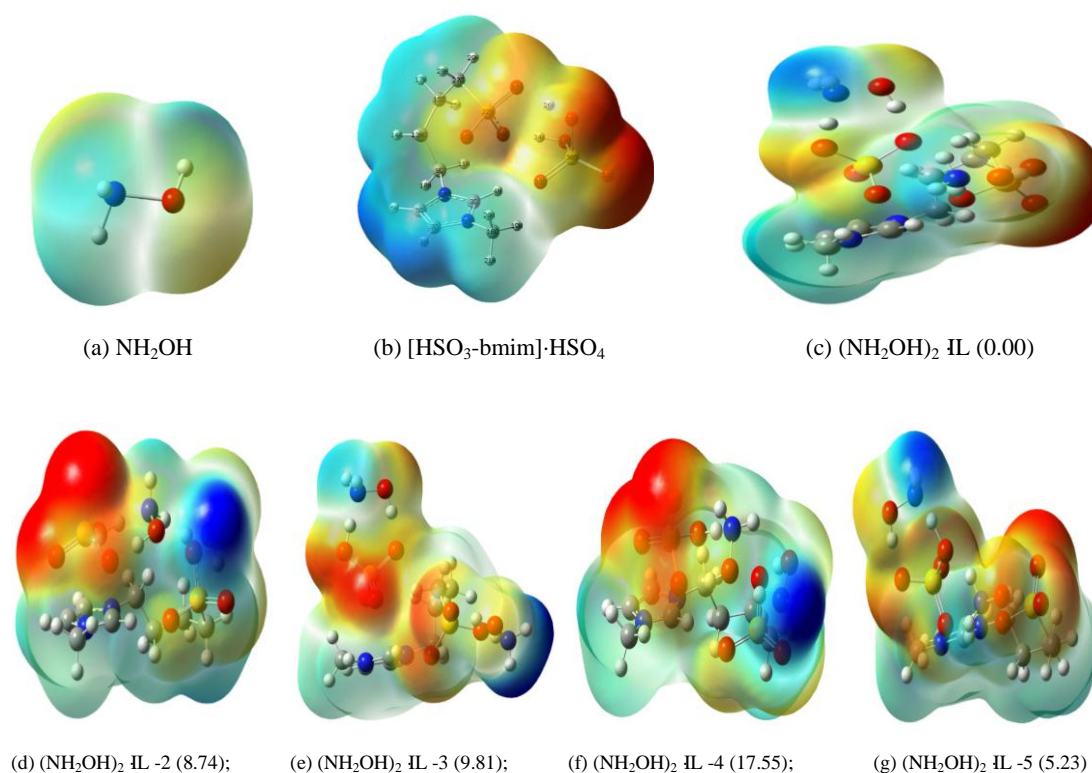


Fig. S3 M062X/6-31++ G electrostatic potential mapped onto the 0.0004 density isosurface (unit: electron Bohr⁻³) for the optimized structures of NH_2OH , $[\text{HSO}_3\text{-bmim}]\cdot\text{HSO}_4$, $(\text{NH}_2\text{OH})_2$ IL and $(\text{NH}_2\text{OH})_2$ -IL-2, -3, -4, -5. The scale spans - 48.96 (red) through 0.0 (green) to 48.96 (blue). Data in brackets is the Gibbs free energy gap with the $(\text{NH}_2\text{OH})_2$ -ILs. unit: kcal/mol.

Table S2 (I) Coordinates of the optimized structure for NH_2OH .

Atoms	X	Y	Z
N	0.699	0	0.14
H	1.067	-0.839	-0.303
H	1.067	0.839	-0.303
O	-0.734	0	-0.139
H	-1.158	0	0.739

Table S2 (II) Coordinates of the optimized structure for $\text{NH}_2\text{OH HCl}$.

Atoms	X	Y	Z
N	1.254	-0.664	0
H	1.666	-1.06	0.845
H	0.098	-0.707	0
O	1.519	0.754	0
H	0.604	1.161	0
Cl	-1.468	0.017	0
H	1.666	-1.06	-0.845

Table S2 (III) Coordinates of the optimized structure for $(\text{NH}_2\text{OH})_2 \text{H}_2\text{SO}_4$.

Atoms	X	Y	Z
O	0	-0.002	-0.083
O	0.947	-0.96	0.878
O	-0.945	0.955	0.881
O	1.027	0.887	-0.985
N	-3.373	0.588	0.362
H	-3.93	0.552	1.215
H	-2.251	0.805	0.615
O	-3.497	-0.718	-0.248
H	-2.554	-0.939	-0.588
O	-1.029	-0.889	-0.984
H	-3.755	1.28	-0.283
O	3.495	0.722	-0.249
H	2.551	0.94	-0.589
N	3.375	-0.583	0.363
H	3.93	-0.544	1.217
H	3.76	-1.275	-0.281
H	2.253	-0.804	0.615

Table S2 (IV) Coordinates of the optimized structure for [HSO₃-bmim]·HSO₄.

Atoms	X	Y	Z
N	-1.262	2.585	-0.258
N	-2.347	0.998	0.752
C	-1.125	1.513	0.532
H	-0.178	1.095	0.85
C	-3.287	1.758	0.064
H	-4.338	1.525	0.089
C	-2.606	2.754	-0.569
H	-2.948	3.555	-1.201
C	-2.63	-0.277	1.43
H	-3.369	-0.077	2.211
H	-1.695	-0.592	1.896
C	-3.141	-1.368	0.449
H	-3.115	-0.966	-0.57
H	-4.186	-1.587	0.685
C	-2.337	-2.693	0.502
H	-1.835	-2.789	1.47
S	-0.137	-1.461	-0.686
O	1.234	-1.962	-1.419
O	0.156	-1.144	0.916
O	-0.929	-0.259	-1.446
H	2.526	-1.133	-1.28
C	-1.311	-2.895	-0.612
H	-1.752	-2.923	-1.61
H	-0.673	-3.764	-0.447
S	3.061	0.369	0.348
O	4.415	1.063	0.795
O	2.588	-0.777	1.523
O	1.756	1.285	0.059
H	1.582	-1.013	1.354

Table S2 (V) Coordinates of the optimized structure for (NH₂OH)₂ IL.

Atoms	X	Y	Z
N	2.717899	1.863719	-1.046421
N	2.947548	0.206318	0.335952
C	2.325381	0.608665	-0.782042
H	1.582316	0.020224	-1.305775
C	3.733597	1.244345	0.817776
H	4.309073	1.151653	1.721978
C	3.591452	2.28534	-0.052785
H	4.020927	3.271378	-0.053307
C	2.672874	-1.060804	1.03605
H	3.61769	-1.41715	1.456666
H	2.356419	-1.788282	0.288003
C	1.607638	-0.840105	2.125982
H	0.937724	-0.040721	1.78957
H	2.101922	-0.475573	3.034616
C	0.786676	-2.09793	2.459706
H	1.397063	-3.00632	2.382679
H	0.449104	-2.034718	3.500971
C	2.225743	2.685465	-2.155348
H	2.923507	2.646186	-2.99359
H	1.238982	2.316539	-2.441567
H	2.118754	3.711658	-1.802461
S	-0.095442	-2.739716	-0.135983
O	0.247277	-1.325368	-0.938327
O	-1.510171	-3.326826	-0.723047
O	1.169052	-3.751408	-0.127841
O	-2.568343	-2.021028	-2.67566
N	-2.014678	-0.790268	-2.174834
H	-1.015831	-0.92997	-1.814619
H	-2.544544	-0.429364	-1.365197
H	-2.015809	-0.11056	-2.933301
H	-2.2152	-2.717987	-2.017363
C	-0.476978	-2.260252	1.62573
H	-1.058082	-1.339028	1.510582
H	-1.108569	-3.083299	1.96606
S	-0.966099	1.623105	-0.175188
O	0.321141	1.712645	0.7927
O	-1.859959	3.052543	-0.029669
O	-0.604716	1.435782	-1.746522
N	-3.649891	2.73761	1.74612
H	-3.40343	3.205497	2.617149
H	-2.646844	2.946887	0.750011
O	-3.788741	1.329067	2.067915
H	-3.145964	0.85746	1.450093
O	-2.049833	0.462986	0.297167
H	-4.564668	3.0541	1.427672

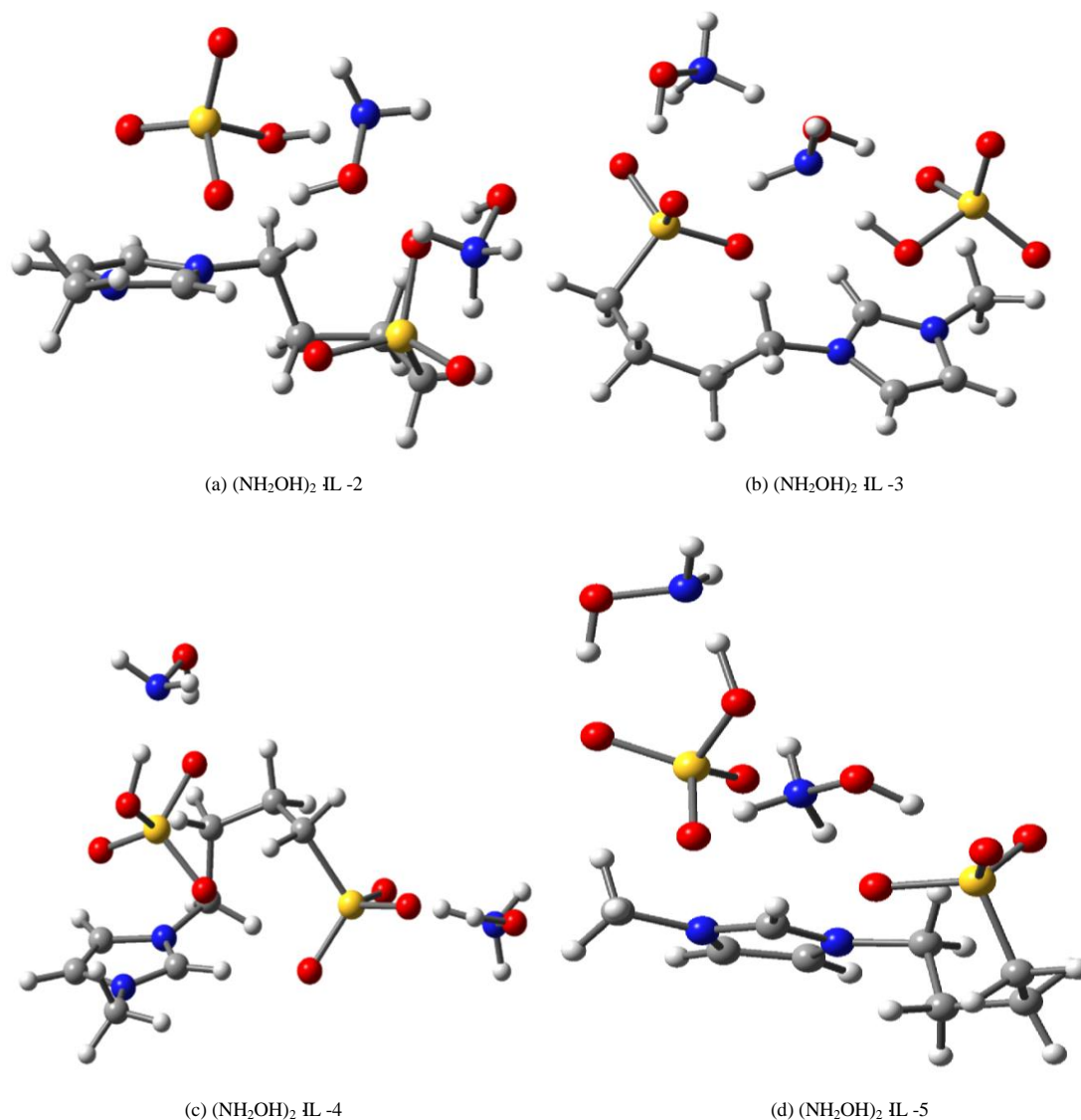


Fig. S4 The optimized structure for $(\text{NH}_2\text{OH})_2 \cdot \text{IL} - 2$ (a) , -3(b) , -4(c) and -5(d)

In situ IR study

The in situ IR spectra of CPL synthesis from CYC and $(\text{NH}_2\text{OH})_2 \cdot \text{IL}$ at different time are shown in Fig. S5. The peak at 1668 cm^{-1} was assigned to the C=O stretching mode in CPL, and the peak at 938 and 892 cm^{-1} were assigned to the N-O stretching mode in cyclohexanone oxime (COX).⁸ However, there was no clear characteristic peak for CYC probably due to the overlap of the C=O stretching mode in CYC and that of the C=N in COX. Thus, only the variation trend of COX and CPL were discussed. As shown in Fig. S5, the absorbance peaks of COX were observed (938 and 892 cm^{-1}) as soon as CYC was added into the reaction system. The peaks of COX increased markedly with the extending of reaction time, and reached a maximum value at 6 min, indicating that CYC reacts easily with $(\text{NH}_2\text{OH})_2 \cdot \text{IL}$ to get COX. Then the peaks decreased gradually as the reaction proceeded. However, the peak corresponding to CPL (1668 cm^{-1}) was not observed at the beginning of the reaction, and it appeared at 6 min, increased gradually with the increase of COX concentration. Then as the reaction proceeded, the peak of CPL became more

intense while those of COX disappeared, indicating that COX was converted into CPL during the present reaction.

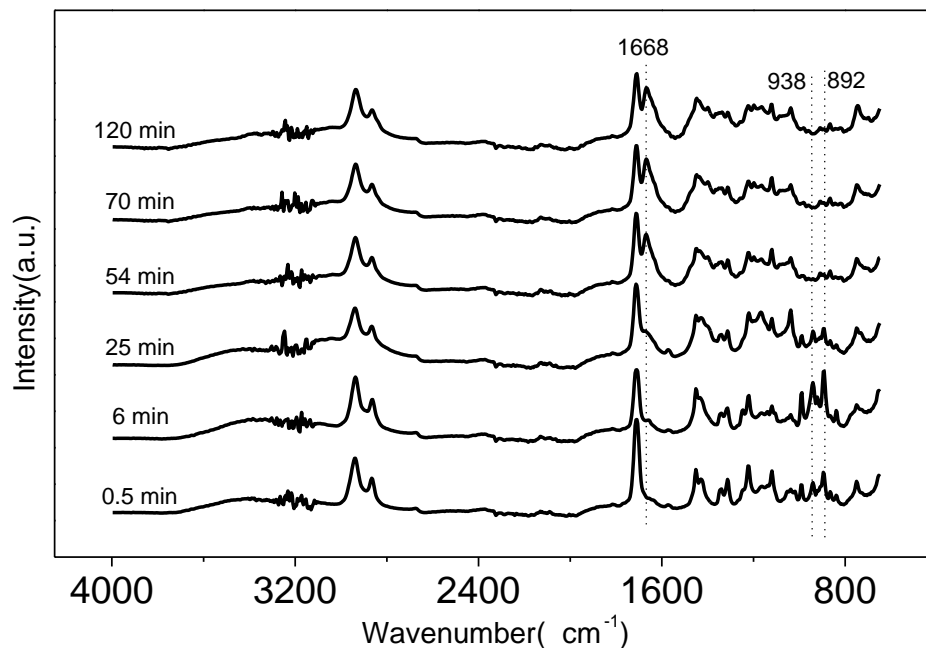
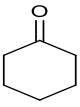
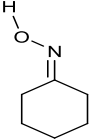
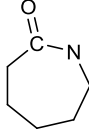


Fig. S5 React-IR spectra of CPL synthesis from CYC and $(\text{NH}_2\text{OH})_2$ IL at different reaction time

Table S3 Calculated and experimentally determined IR spectra values for the substance involved with their assignment (wavenumber in cm^{-1})

Substance	Experimental value	Calculated value		Assignment
		Unscaled	Scaled ^a	
	1709-1712	1754	1710	$\nu(\text{C}=\text{O})$
	892	911	888	$\nu(\text{N}-\text{O})$
	938	951	927	$\nu(\text{N}-\text{O})$
	1709-1712	1765	1721	$\nu(\text{C}=\text{N})$
	1668	1717	1674	$\nu(\text{C}=\text{O})$

a: Scaled by frequency factor 0.975.

For the important species involved, vibrational assignments were carried out with support of DFT calculations using the M062X method with a 6-31++g basis set. The calculated and experimental values for the IR vibrational frequencies are listed in Table S3. In general, the absorption frequencies obtained from our experiments agreed well with the calculation (their coordinates are shown in Table S4I-III).

Table S4 (I) Coordinates of the optimized structure for CYC.

Atoms	X	Y	Z
C	-1.00847100	-1.26257200	-0.29107100
C	0.39040600	-1.28179200	0.35877100
C	1.14096400	0.00000000	0.07609100
C	0.39040600	1.28179200	0.35877200
C	-1.00847100	1.26257200	-0.29107100
C	-1.78513200	0.00000000	0.10508200
H	0.27389800	-1.37299800	1.44910300
H	0.99321100	-2.12424700	0.01096800
H	-0.89927000	-1.29308500	-1.38332300
H	-1.55908300	-2.16325300	-0.00032800
H	0.27389800	1.37299800	1.44910300
H	0.99321100	2.12424700	0.01096800
H	-1.55908300	2.16325300	-0.00032800
H	-0.89927000	1.29308500	-1.38332300
H	-1.95417000	0.00000000	1.19171700
H	-2.77170100	0.00000000	-0.37133100
O	2.29876900	0.00000000	-0.35908400

Table S4 (II) Coordinates of the optimized structure for COX.

Atoms	X	Y	Z
C	-1.67865200	-1.01494000	-0.41252100
C	-0.42314200	-1.40019300	0.39321100
C	0.63730800	-0.34112600	0.24521800
C	0.22346300	1.07539400	0.53841800
C	-1.04848700	1.42971400	-0.26001400
C	-2.15962900	0.39392800	-0.03820600
H	-0.69198900	-1.47922100	1.45685600
H	-0.02049400	-2.36537500	0.07519200
H	-1.43994100	-1.04529400	-1.48416200
H	-2.46927400	-1.75240900	-0.23656700
H	0.00335600	1.15056700	1.61364900
H	1.03951200	1.76287100	0.31464100
H	-1.39108100	2.42937300	0.02820400
H	-0.79850600	1.47023800	-1.32849900
H	-2.46292700	0.40571600	1.01909800
H	-3.04498200	0.65951700	-0.62672800
N	1.79866400	-0.72898600	-0.14552800
O	2.72804700	0.38076000	-0.25684000
H	3.55613000	-0.03582500	-0.55491100

Table S4 (III) Coordinates of the optimized structure for CPL.

Atoms	X	Y	Z
C	1.38166100	-0.03335800	0.03146300
C	-0.64132300	-1.49442000	0.41904500
C	0.62496300	1.14903600	0.59497200
C	-1.72140400	-0.75730800	-0.38303700
C	-0.58622500	1.56110400	-0.26775900
C	-1.85066900	0.72705600	-0.02152400
H	-0.73932800	-1.24688600	1.48544800
H	-1.49839600	-0.86840000	-1.45201000
H	1.35079800	1.96254900	0.64647600
H	-0.30583500	1.51391600	-1.32837200
H	-0.78951700	-2.57370700	0.33123400
H	0.29225600	0.93220100	1.61964000
H	-2.68467300	-1.24999400	-0.20003500
H	-0.81637000	2.61054300	-0.05191400
H	-2.67972200	1.16184200	-0.59275700
H	-2.12656300	0.80996200	1.04060800
O	2.55489900	0.07628200	-0.38241200
N	0.72277100	-1.22703800	-0.03428800
H	1.25674600	-1.98568900	-0.43796000

1 M. I. Fernandez, M. Canle, M. V. Garcia and J. A. Santaballa, *Chem. Phys. Lett.*, 2010, **490**, 159.

2 (a) D. Amariei, L. Courthe ôux, S. Rossignol and C. Kappenstein, *Chem. Eng. Prog.*, 2007, **46**, 165; (b) *US Pat.*, 5266290, 1993.

3 Y. L. Geng, L. Y. Hu, X. Q. Zhao, H. L. An and Y. J. Wang, *Chin. J. Chem. Eng.*, 2009, **17**(5), 756.

4 M. J. Frisch, G. W. Trucks, H. B. Schlegel, etc., Gaussian 09, Revision D.01, Gaussian, Inc., Wallingford CT, 2009.

5 (a) Y. Zhao and D. G. Truhlar, *Theor. Chem. Account.*, 2008, **120**, 215; (b) C. Q. Chu, H. T. Zhao, Y. Y. Qi and F. Xin, *J. Mol. Model.*, 2013, **19**, 2217; (c) H. Roohi and S. Khyrkhah, *J. Mol. Liq.*, 2013, **177**, 119; (d) Y. Valadbeigi, H. Farrokhpour and M. Tabrizchi, *Phys. Lett. A.*, 2014, **378**, 777.

6 G. L. Borosky, T. Okazaki and K. K. Laali, *Eur. J. Org. Chem.*, 2011, **2011**, 1771.

7 W. M. Reichert, P. C. Trulove and H. C. De Long, *Acta Crystallogr. Sect. E: Struct. Rep. Online*, 2010, **E66**, o591.

8 S. F. Weng, *Fourier Transform Infrared Spectrometer*, Beijing, Chemical Industry Press, 2005, 255, 272.